

IMPROVING GNSS POSITIONING RELIABILITY AND ACCURACY BASED ON FACTOR GRAPH OPTIMIZATION IN URBAN ENVIRONMENT

Y. Zhang¹, F. Zhu^{1*}, X. Zhang²

¹ School of Geodesy and Geomatics, Wuhan University, Wuhan 430079, China – (officialtai, fzhu)@whu.edu.cn

² Chinese Antarctic Center of Surveying and Mapping, Wuhan University, Wuhan 430079, China – xhzhang@sgg.whu.edu.cn

KEYWORDS: Factor Graph Optimization, Single-differenced Model, Urban Environments, Outlier Detection, GNSS Positioning.

ABSTRACT:

Global navigation satellite system (GNSS) can provide global, precise, and continuous positioning in open-sky environments. However, urban environments with frequent outliers and cycle slips degrade the traditional Extended Kalman Filter (EKF) positioning performance. The susceptibility of EKF to outliers is attributed to its inherent structure. To mitigate, the GNSS positioning based on the Factor Graph Optimization (FGO) structure is adopted. FGO can enhance time correlation among observations and enable the updating of historical information, thereby improving resistance against outliers. In this study, we proposed a single-differenced GNSS-FGO model instead of the double-differenced model to preserve the sparsity of FGO, and outlier detection and PAR methods are employed to ensure urban positioning performance. To evaluate the proposed structure, experiments are conducted in both urban and open-sky environments. The results demonstrate the improvement of positioning accuracy and reliability, compared to EKF.

1. INTRODUCTION

Global navigation satellite system (GNSS) has been widely used in various application scenarios to introduce precise, global-referenced positions for navigation systems. Generally, the Extended Kalman Filter (EKF) is a classic choice for the GNSS algorithm, which can provide high-precision positioning in open-sky environments (Takasu and Yasuda, 2009). However, challenging environments, such as urban canyons, with poor data quality due to outliers, non-line-of-sight (NLOS), multipath signals, and cycle slips, will largely degrade the reliability and accuracy of GNSS positioning. The filtering method relies solely on a priori information of the state to reserve historical observations via the dynamic model, yet linearization points of the historical states will remain constant. Ineffective detection of outliers can raise large linearization point errors and, consequently, pollute the priori information, threatening GNSS positioning accuracy and reliability. On the other hand, the factor graph was first proposed by Kschischang (2001) and then introduced into the robotics field as an optimal estimation method (Dellaert and Kaess, 2006), Factor Graph Optimization (FGO). In contrast to EKF, all historical observations can be considered simultaneously in FGO estimation, offering several theoretical advantages. Firstly, the FGO method enables updating the information of previous epochs by current observations such as data quality. Secondly, the linearization points of historical observations vary through multiple iterations, facilitating in dealing nonlinear problem. Additionally, the graph optimization structure enhances time correlation across epochs, thereby improving resistance against outliers. From the perspective of graph optimization, EKF can be roughly seen as a sliding-window FGO with a window size of 1.

The study of GNSS positioning based on graph optimization was first carried out by Sünderhauf and Protzel (2012). Suzuki (2021; 2022) has achieved first place in the consecutive Google Smartphone Decimeter Challenge (GSDC) using the factor graph optimization model, showcasing the feasibility of

employing FGO in solving GNSS positioning problems. Watson and Gross (2018) have found that the graph optimization provided a substantial RSOS positioning error reduction during the initial PPP convergence period compared to the traditional EKF-PPP. And his another work shows that traditional M-Estimators can aid graph optimization in adverse environments, proved on pseudorange measurements (Watson and Gross, 2017). Wen and Hsu (2021) have constructed a factor graph model for RTK positioning based on double-difference measurements and analyzed the FGO performance through the urban canyon dataset by the positioning results. Yan et al. (2023) found that FGO had a lower degree of nonlinearity than EKF. And time difference carrier phase (TDCP) is utilized to enhance time correlation (Bai et al., 2022; Jiang et al., 2022). There are also works on tight integration of GNSS with other sensors based on FGO (Cao et al., 2022; Li et al., 2023; Niu et al., 2023).

Among the various models of GNSS-FGO, real-time kinematic (RTK) positioning is the most prevalent in engineering applications, due to its effectiveness in eliminating most GNSS errors through the double-difference (DD) model. However, the current FGO-RTK structures primarily rely on DD measurements, the correlation of which can hinder the sparsity of FGO and present difficulty in implementation. Moreover, there is limited research addressing the outlier detection procedure in FGO, a critical aspect for accurate positioning in urban environments. To address this issue, this paper presents an FGO-GNSS structure based on the single-differenced model with fixed solutions to improve GNSS positioning performance in urban environments, as shown in Figure 1. The contributions of this paper are listed as follows:

- 1) An FGO-GNSS structure based on the SD model is developed, leveraging pseudorange and carrier phase measurements.
- 2) To ensure the positioning performance of urban environments, an outlier detection procedure is

* Corresponding author

- implemented and the partial ambiguity resolution method is adopted.
- 3) The proposed structure is evaluated in urban and open-sky environments datasets and the quality of ambiguity resolution is examined in detail.

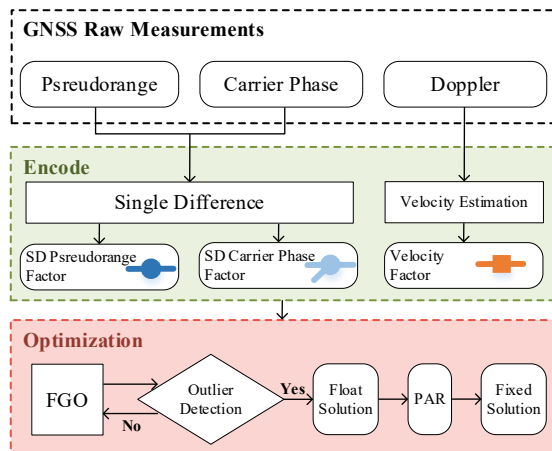


Figure 1. Algorithm architecture

2. METHODOLOGY

2.1 Factor Graph Optimization

As a probabilistic graphical model, factor graph represents the optimization problem concisely. Factor graph is an undirected bipartite graph, consisting of two types of nodes: the variable node X encoding state to be estimated and the factor node $\phi(X)$ encoding measurements cost function, with edge connecting correlated nodes. The maximum a posteriori (MAP) problem comes down to maximizing the product of all factor nodes (Dellaert and Kaess, 2017):

$$X^{MAP} = \underset{X}{\operatorname{argmax}} \phi(X) = \underset{X}{\operatorname{argmax}} \prod_i \phi_i(X_i) \quad (1)$$

where $\phi(X)$ stands for the probability density of the corresponding measurement z_i . However, it is difficult to obtain the true probability density in practical application, for which $\phi(X)$ is always assumed normally distributed:

$$z_i \sim N(h_i(X_i), \Sigma_i) \quad (2)$$

where $h_i(X_i)$ denotes the measurement model of z_i . Σ_i denotes the measurement covariance. Thus, equation (1) can be transformed into minimizing the sum of nonlinear least-squares:

$$X^{MAP} = \underset{X}{\operatorname{argmin}} \sum_i \|z_i - h_i(X_i)\|_{\Sigma_i}^2 \quad (3)$$

where $\|\cdot\|_{\Sigma_i}^2$ denotes the squared Mahalanobis distance. From the perspective of estimation, the Kalman Filter can be considered as generalized least-squares. Therefore, updating historical information is the primary distinction between EKF and FGO, provided consistent information and measurement models.

2.2 Single-Differenced Model

It is essential that the factors in the graph be uncorrelated from one another. However, DD measurements of the same frequency and the same satellite constellation tend to be correlated due to between-satellite single differencing, as shown in Figure 2. Therefore, the DD measurements be incorporated as a whole factor, which may bring dense matrices into optimization, adversely impacting sparsity. To address this issue, this paper adopts the SD model. By between-receiver single differencing, we can also eliminate a majority of GNSS errors arising from satellite and propagation.

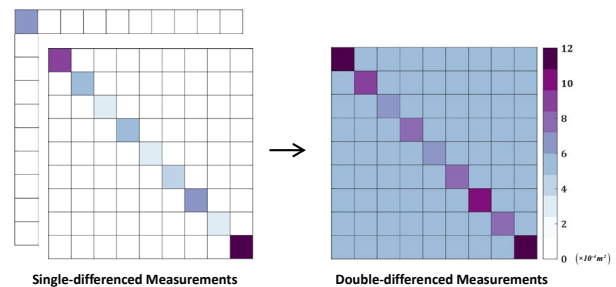


Figure 2. Illustration of single-differenced measurements sparsity

Figure 3 depicts the graph structure of the proposed method, note that there should be multiple factors and variables in the graph, which are omitted for brevity. The estimated state variables at epoch n are represented as follows:

$$X^* = \{X_1, X_2, \dots, X_n, \Delta N_1^1, \Delta N_1^2, \dots, \Delta N_f^S\} \quad (4)$$

$$X_k = [x_k \quad \delta t_k]^T$$

where X^* denotes the state space corresponding to the graph model. ΔN_f^S denotes SD ambiguity received from satellite S on frequency f . This paper considers ambiguity ΔN_f^S as a constant across different epochs without cycle slip, owing to the nature of carrier phase measurements. And it can also improve the time correlation among measurements. X_k denotes the state at epoch k , including position x_k and single-differenced receiver clock bias δt_k . The estimation of δt_k is required, as errors originating from the receiver have not been eliminated. The SD measurement model is represented as follows:

$$\begin{cases} \Delta L_k^{i,f} = \Delta \rho^i + \lambda_f \Delta N_f^S + \delta t_k \\ \Delta P_k^{i,f} = \Delta \rho^i + \delta t_k \end{cases} \quad (5)$$

where pseudorange and carrier phase from satellite i on frequency f are respectively denoted as $\Delta P_k^{i,f}$ and $\Delta L_k^{i,f}$. $\Delta \rho^i$ is the single-differenced geometric satellite-to-receiver distance. And SD ambiguity ΔN_f^S is estimated, capable of handling the hand-over of reference satellite. Hence, the cost function of single-differenced measurements is expressed as:

$$\begin{aligned} \|e_k^{\Delta L_i}\|_{\Sigma_L}^2 &= \|\Delta L_k^{i,f} - h^L(x_k, \Delta N_f^S, \delta t_k)\|_{\Sigma_L}^2 \\ \|e_k^{\Delta P_i}\|_{\Sigma_P}^2 &= \|\Delta P_k^{i,f} - h^P(x_k, \delta t_k)\|_{\Sigma_P}^2 \end{aligned} \quad (6)$$

To enhance the time correlation, velocity v_k can be derived from doppler measurements by least square. And velocity factor is adopted to constrain adjacent position states.

$$\|e_k^v\|_{\Sigma_v}^2 = \|v_k - h^v(x_k, x_{k-1})\|_{\Sigma_v}^2 \quad (7)$$

Including three types of factors, the final cost function of the proposed method is represented as follows:

$$X^* = \underset{X^*}{\operatorname{argmin}} \sum_{i,k} \|e_k^{\Delta_i}\|_{\Sigma_L}^2 + \|e_k^{\Delta_p}\|_{\Sigma_p}^2 + \|e_k^v\|_{\Sigma_v}^2 \quad (8)$$

For high-precision positioning, it is critical to achieve integer ambiguity resolution (AR). So after the float solution is estimated by FGO, the float SD ambiguity associated to the current epoch k will be selected out of the state space and subjected to between-satellite single differencing to obtain float DD ambiguity. This paper applies the Least-squares AMBiguity Decorrelation Adjustment (LAMBDA) algorithm to solve the AR problem (Teunissen, 1995), independent of FGO. Partial ambiguity resolution is also employed to ensure reliability in the urban environment.

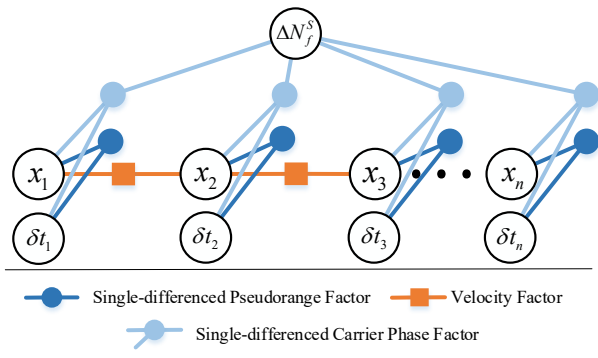


Figure 3. Graph structure for SD-RTK

2.3 Outlier Detection

In urban environments, frequent cycle slips and outliers can be hazardous to the reliability and accuracy of GNSS positioning. In addition to regular prior detection, a post outlier detection with graph structure is implemented to ensure robust positioning performance of the proposed structure. Traditional EKF can only detect outliers of the current epoch. With FGO, we can detect outliers of epochs inside the sliding window to enhance data redundancy. It is also possible that we detect previous missing outliers together with current observations. The test statistics of outlier detection can be formulated as follows (Teunissen and Montenbruck, 2017):

$$\|r\|_{D_z}^2 = r^T D_z^{-1} r < \chi_\alpha^2(q, 0) \quad (9)$$

where r denotes the residual vector of observed measurements. D_z denotes the measurement covariance. $\chi_\alpha^2(q, 0)$ is the threshold computed from the central Chi-squared distribution with q degrees of freedom.

If the test is successful, the measurements are deemed free of outliers. In the event of a test failure, the biggest residual is recognized as an outlier under mean drift model assumptions,

and a re-optimization is conducted to re-linearize the state X^* . As shown in Figure 4, the detected SD pseudorange factor will be reweighted to zero, and the detected SD carrier phase factor will be considered as cycle slips. In the event of a cycle slip occurring, a new variable ΔN_f^s will be introduced into the graph to distinguish it from ΔN_f^s .

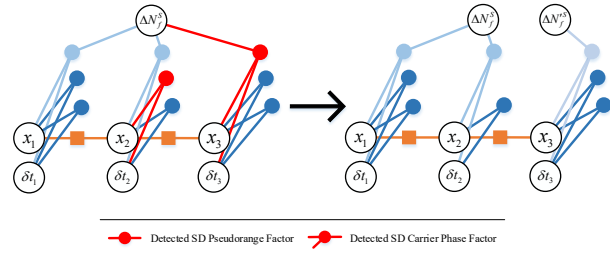


Figure 4. Outlier detection of FGO

3. EXPERIMENTS

To evaluate the proposed framework, a comparison has been conducted between FGO and standard EKF-RTK. The same processing strategy is applied for both methods to ensure the validity of the results as shown in Table 1.

Item	Strategy
Measurements	GPS: L1/L2
	BDS: B1/B2
	GAL: E1/E5a
	GLO: L1/L2
	QZS: L1/L2
Ephemeris	broadcast ephemeris
Dynamic model/ Constraint factor	GNSS velocity
Elevation mask angle	15°
Stochastic model	Elevation-dependent model
Outlier detection	Chi-square test
Phase Ambiguities	PAR

Table 1. Processing strategy

As shown in Figure 5, the vehicle experiment is carried out in urban environments, with a total length of over 8km and a duration of about 1200s. The trajectory has covered typical urban scenes like avenues, urban canyons, and bridges, which can lead to a considerable number of outliers and frequent signal interruptions. The dataset is collected by NovAtel SPAN at a frequency of 1 Hz and a post-process GNSS/INS integration solution is adopted as the reference.

Figure 6 presents the trajectories of FGO and EKF. Overall, the FGO provides a smoother and more accurate trajectory over EKF, thanks to the time correlation factor. While both are unable to obtain fixed solutions in the deep urban area due to GNSS obstruction, more reliable positioning is achieved by FGO. Furthermore, Figure 7 and Figure 8 give the position error sequence of FGO and EKF in the east-north-up (ENU) frame, respectively. FGO is apparently less affected by the outliers and presents an improvement in positioning accuracy and reliability.

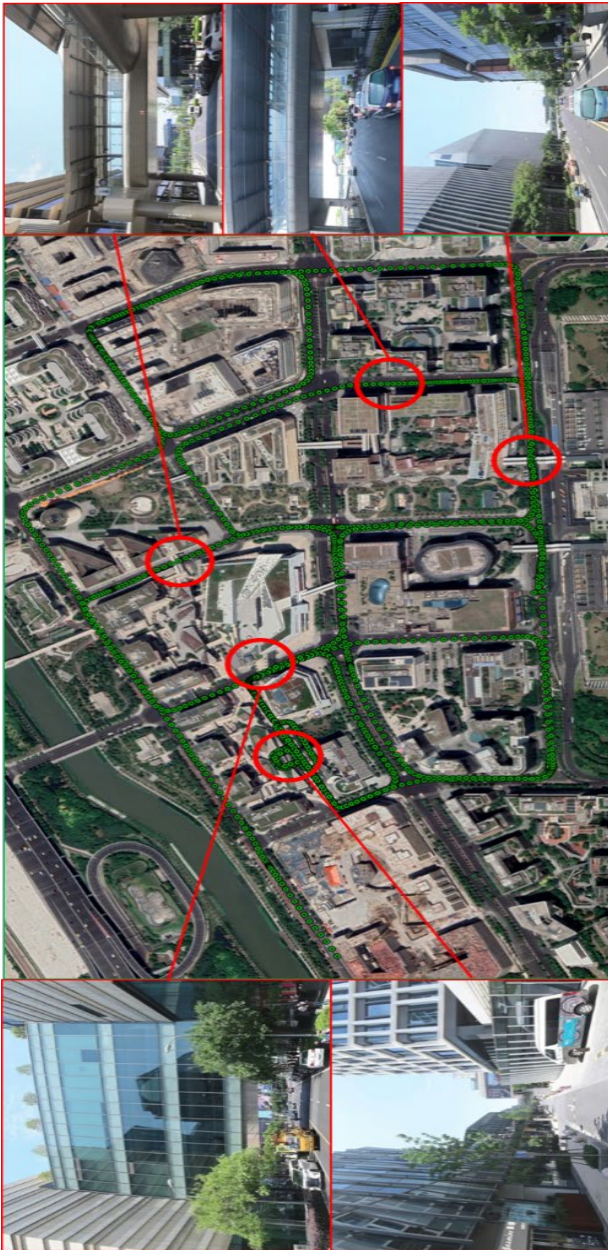


Figure 5. Route and environment of urban experiment

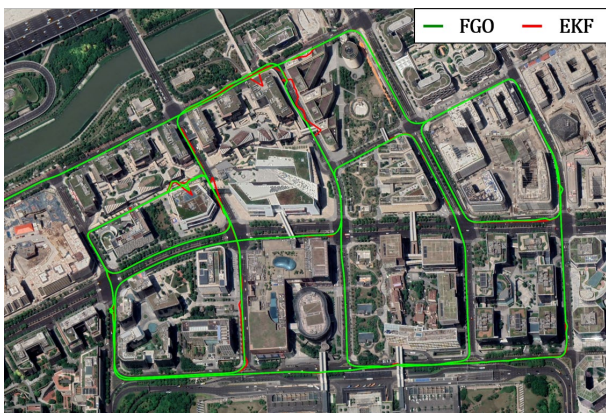


Figure 6. Trajectories of urban experiment

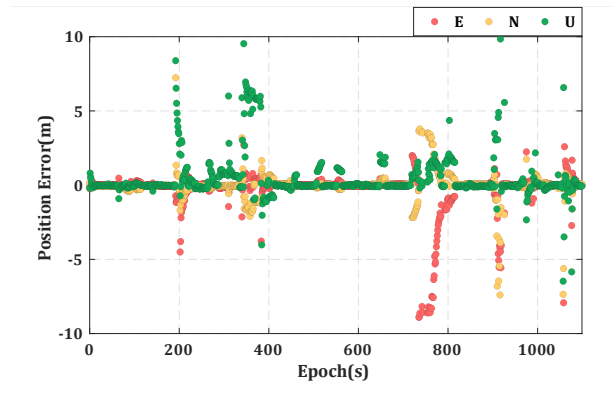


Figure 7. Positioning error sequence of FGO

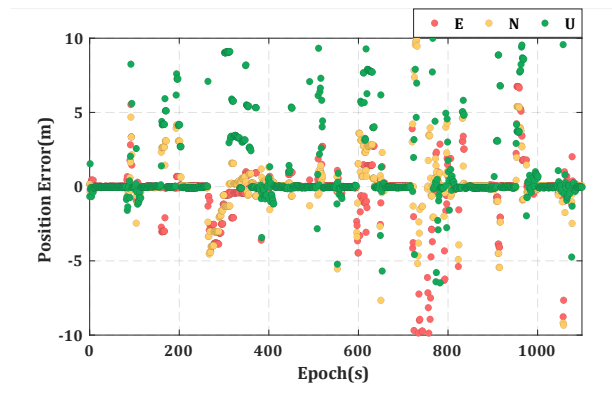


Figure 8. Position error sequence of EKF

Furthermore, the statistics of position errors for four methods, EKF-FLO, EKF-AR, FGO-FLO, FGO-AR are summarized in Table 2 respectively. Due to the better capability of outlier detection, the RMSEs of fixed solution drop from 2.30, 1.89, and 6.42 m to 1.45, 0.93, and 1.67 m in the ENU directions. The cumulative distribution of position errors is shown in Figure 9. EKF and FGO both can provide reliable positioning under normal conditions. Yet the maximum and one sigma statistics show that FGO remains better robust under outliers. due to a better float solution, FGO-AR gives the best performance. This improvement indicates the effectiveness of the proposed framework.

Float Solution	FGO-FLO			EKF-AR		
	E	N	U	E	N	U
1 σ (m)	0.47	0.47	1.58	0.63	0.49	2.61
RMSE(m)	1.46	1.04	2.31	2.36	1.93	6.68
MAX(m)	11.36	11.80	13.65	20.55	27.11	40.01
Fixed Solution	FGO-AR			EKF-AR		
	E	N	U	E	N	U
1 σ (m)	0.07	0.09	0.24	0.16	0.22	0.56
RMSE(m)	1.45	0.93	1.67	2.30	1.89	6.42
MAX(m)	11.36	11.80	13.65	20.55	27.11	40.01

Table 2. Statistics of position errors

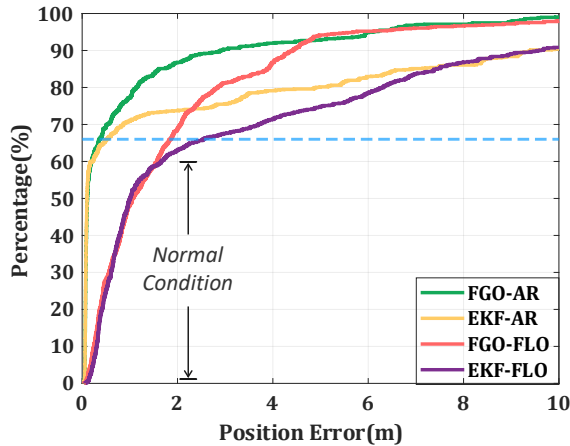
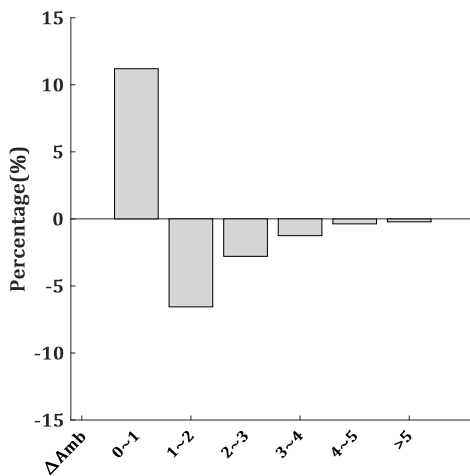


Figure 9. Cumulative distribution of position errors

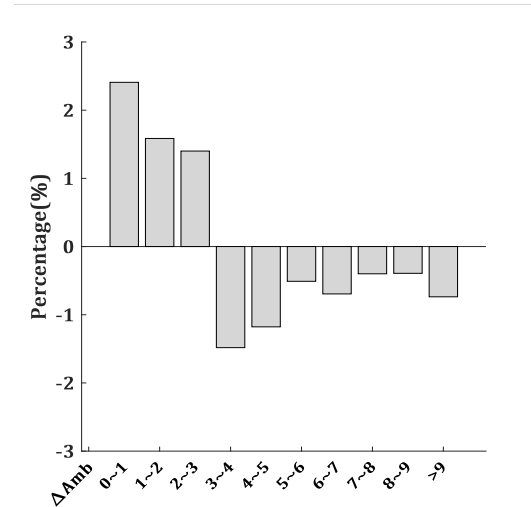
To further evaluate the AR performance of the proposed structure, an additional experiment is conducted in open-sky environments. Table 3 presents the evaluation index of AR in two experiments. The open-sky data reveals notable improvements in the mean ratio and Ambiguity Dilution of Precision (ADOP), increasing from 36.4 and 0.0273 cycles to 44.7 and 0.0267 cycles, respectively., which indicates better quality of fixed solution and AR performance. Moreover, the ambiguity residuals are formulated as follows:

$$\Delta a = |\Delta \tilde{a} - \Delta \hat{a}| \quad (10)$$

where $\Delta \tilde{a}$ and $\Delta \hat{a}$ denote fixed and float DD ambiguities respectively. Figure 10 is presented to provide an intuitive comparison of the Δa distribution between both methods. The deviation of the distribution is determined by subtracting the distribution of Δa_{EKF} from the distribution of Δa_{FGO} . As can be seen from the figure, the FGO outperforms EKF with a more centralized distribution in the open-sky dataset, which contributes to better AR performance. Consistent with the open-sky dataset, slight improvement can be seen from the urban dataset. The main reason is that signal interruptions lead to the frequent reset of ambiguity, lessening the impact of the FGO.



(a) Open-sky dataset



(b) Urban dataset

Figure 10. Deviation of ambiguity residual distribution

Dataset	Method	\overline{ratio}	$\overline{ADOP}(cyc)$
Open-sky	FGO	44.7	0.0267
	EKF	36.4	0.0273
Urban	FGO	8.62	0.0570
	EKF	7.39	0.0671

Table 3. Statistics of ambiguity resolution

4. CONCLUSIONS

Urban canyons, with frequent outliers, and cycle slips, will largely degrade the reliability and accuracy of GNSS positioning. This paper develops an FGO-GNSS structure based on the single-differenced model adopting pseudorange and carrier phase measurements. Outlier detection and PAR methods are employed to improve performance in urban environments. In the context of consistent processing strategies, a comparative analysis is conducted between FGO and EKF through experiments in urban and open-sky environments. The results of both experiments reveal that FGO exhibits improvements in ratio and ADOP, showing better quality of ambiguity resolution. In the urban experiment, the position RMSEs exhibit a notable decrease from 2.30 m, 1.89 m, and 6.42 m to 1.45 m, 0.93 m, and 1.67 m in the ENU directions and a reduction in maximum errors. The result indicates that the proposed structure can evidently advance the performance of AR and outlier detection, leading to the improvement of positioning accuracy and reliability. However, the signal interruption situation can be difficult for GNSS, thus our future work will focus on fusing more sensors such as inertial to strengthen the positioning capability.

REFERENCES

Bai, X., Wen, W., Hsu, L.-T., 2022. Time-Correlated Window-Carrier-Phase-Aided GNSS Positioning Using Factor Graph Optimization for Urban Positioning. IEEE Trans. Aerosp. Electron. Syst. 58, 3370–3384. doi.org/10.1109/TAES.2022.3149730

Cao, S., Lu, X., Shen, S., 2022. GVINS: Tightly Coupled GNSS–Visual–Inertial Fusion for Smooth and Consistent State

- Estimation. *IEEE Transactions on Robotics* 38, 2004–2021. doi.org/10.1109/TRO.2021.3133730
- Dellaert, F., Kaess, M., 2017. Factor Graphs for Robot Perception. *ROB* 6, 1–139. doi.org/10.1561/23000000043
- Dellaert, F., Kaess, M., 2006. Square Root SAM: Simultaneous Localization and Mapping via Square Root Information Smoothing. *The International Journal of Robotics Research* 25, 1181–1203. doi.org/10.1177/0278364906072768
- Jiang, Y., Gao, Yuting, Ding, W., Gao, Yang, 2022. GNSS precise positioning for smartphones based on the integration of factor graph optimization and solution separation. *Measurement* 203, 111924. doi.org/10.1016/j.measurement.2022.111924
- Kschischang, F.R., Frey, B.J., Loeliger, H.-A., 2001. Factor graphs and the sum-product algorithm. *IEEE Trans. Inform. Theory* 47, 498–519. doi.org/10.1109/18.910572
- Li, X., Yu, H., Wang, X., Li, S., Zhou, Y., Chang, H., 2023. FGO-GIL: Factor graph optimization-based GNSS RTK/INS/LiDAR Tightly Coupled Integration for precise and continuous navigation. *IEEE Sensors Journal* 1–1. doi.org/10.1109/JSEN.2023.3278723
- Niu, X., Tang, H., Zhang, T., Fan, J., Liu, J., 2023. IC-GVINS: A Robust, Real-Time, INS-Centric GNSS-Visual-Inertial Navigation System. *IEEE Robot. Autom. Lett.* 8, 216–223. doi.org/10.1109/LRA.2022.3224367
- Sünderhauf, N., Protzel, P., 2012. Towards robust graphical models for GNSS-based localization in urban environments, in: *International Multi-Conference on Systems, Signals & Devices*. Presented at the International Multi-Conference on Systems, Signals & Devices, pp. 1–6. doi.org/10.1109/SSD.2012.6198059
- Suzuki, T., 2022. 1st Place Winner of the Smartphone Decimeter Challenge: Two-Step Optimization of Velocity and Position Using Smartphone's Carrier Phase Observations. Presented at the Proceedings of the 35th International Technical Meeting of the Satellite Division of The Institute of Navigation (ION GNSS+ 2022), pp. 2276–2286. doi.org/10.33012/2022.18377
- Suzuki, T., 2021. First Place Award Winner of the Smartphone Decimeter Challenge: Global Optimization of Position and Velocity by Factor Graph Optimization. Presented at the 34th International Technical Meeting of the Satellite Division of The Institute of Navigation (ION GNSS+ 2021), St. Louis, Missouri, pp. 2974–2985. doi.org/10.33012/2021.18109
- Takasu, T., Yasuda, A., 2009. Development of the low-cost RTK-GPS receiver with an open source program package RTKLIB, in: *International Symposium on GPS/GNSS*. International Convention Center Jeju Korea Seogwipo-si, Korea, pp. 1–6.
- Teunissen, P.J.G., 1995. The least-squares ambiguity decorrelation adjustment: a method for fast GPS integer ambiguity estimation. *Journal of Geodesy* 70, 65–82. doi.org/10.1007/BF00863419
- Teunissen, P.J.G., Montenbruck, O. (Eds.), 2017. *Springer Handbook of Global Navigation Satellite Systems*. Springer International Publishing, Cham. doi.org/10.1007/978-3-319-42928-1
- Watson, R.M., Gross, J.N., 2018. Evaluation of kinematic precise point positioning convergence with an incremental graph optimizer, in: *2018 IEEE/ION Position, Location and Navigation Symposium (PLANS)*. Presented at the 2018 IEEE/ION Position, Location and Navigation Symposium (PLANS), IEEE, Monterey, CA, pp. 589–596. doi.org/10.1109/PLANS.2018.8373431
- Watson, R.M., Gross, J.N., 2017. Robust Navigation In GNSS Degraded Environment Using Graph Optimization. Presented at the Proceedings of the 30th International Technical Meeting of the Satellite Division of The Institute of Navigation (ION GNSS+ 2017), pp. 2906–2918. doi.org/10.33012/2017.15164
- Wen, W., Hsu, L.-T., 2021. Towards Robust GNSS Positioning and Real-time Kinematic Using Factor Graph Optimization, in: *2021 IEEE International Conference on Robotics and Automation (ICRA)*. Presented at the 2021 IEEE International Conference on Robotics and Automation (ICRA), IEEE, Xi'an, China, pp. 5884–5890. doi.org/10.1109/ICRA48506.2021.9562037
- Yan, S., Lü, S., Liu, G., Zhan, Y., Lou, J., Zhang, R., 2023. Real-time Kinematic Positioning Algorithm in Graphical State Space. Presented at the 2023 International Technical Meeting of The Institute of Navigation, Long Beach, California, pp. 637–648. doi.org/10.33012/2023.18676